

Inferring entropy production in many-body systems using nonequilibrium MaxEnt

Miguel Aguilera,^{1,2,*} Sosuke Ito,^{3,4} and Artemy Kolchinsky^{5,3,*}

¹BCAM – Basque Center for Applied Mathematics, 48009 Bilbao, Spain

²IKERBASQUE, Basque Foundation for Science, 48009 Bilbao, Spain

³Universal Biology Institute, The University of Tokyo, 7-3-1 Hongo, Bunkyo-ku, Tokyo 113-0033, Japan

⁴Department of Physics, The University of Tokyo, 7-3-1 Hongo, Bunkyo-ku, Tokyo 113-0033, Japan

⁵ICREA-Complex Systems Lab, Universitat Pompeu Fabra, 08003 Barcelona, Spain

We propose a method for inferring entropy production (EP) in high-dimensional stochastic systems, including many-body systems and non-Markovian systems with long memory. Standard techniques for estimating EP become intractable in such systems due to computational and statistical limitations. We infer trajectory-level EP and lower bounds on average EP by exploiting a nonequilibrium analogue of the Maximum Entropy principle, along with convex duality. Our approach uses only samples of trajectory observables (such as spatiotemporal correlation functions). It does not require reconstruction of high-dimensional probability distributions or rate matrices, nor any special assumptions such as discrete states or multipartite dynamics. It may be used to compute a hierarchical decomposition of EP, reflecting contributions from different kinds of interactions, and it has an intuitive physical interpretation as a thermodynamic uncertainty relation. We demonstrate its numerical performance on a disordered nonequilibrium spin model with 1000 spins and a large neural spike-train dataset.

The central quantity of interest in nonequilibrium thermodynamics is *entropy production* (EP) [1]. EP characterizes departure from thermodynamic equilibrium in microscopic physical systems, where it quantifies the dissipation of thermodynamic free energy. More generally, EP provides an information-theoretic measure of temporal irreversibility, including in meso- and macroscopic systems [2–5]. There is great interest in quantifying EP in high-dimensional complex systems with many degrees of freedom and/or long non-Markovian memory, such as nonequilibrium disordered networks [6], biological active matter [7, 8], and neural systems [9–13], but this is computationally and statistically difficult. Standard methods require reconstruction of trajectory probability distributions, an intractable problem for systems with many spatiotemporal degrees of freedom.

In this paper, we propose a method to infer EP in high-dimensional stochastic systems. To do so, we introduce a variational principle that is the nonequilibrium analogue of the well-known Maximum Entropy Principle (MaxEnt) from equilibrium statistical physics. The dual form of this variational principle leads to a tractable optimization problem whose solution provides an approximation of trajectory-level EP and a lower bound on the average EP — directly from trajectory samples and without explicit knowledge of trajectory probabilities. The dual principle also provides a higher-order thermodynamic uncertainty relation (TUR) [14, 15], which we use to derive further simple bounds on EP.

Entropy production.— We consider a nonequilibrium stochastic system measured at discrete time points. The system’s (continuous or discrete) state at any given time is a vector $\mathbf{x}_t = (x_{1,t}, x_{2,t}, \dots, x_{N,t})$ of dimension N . These dimensions may represent physical degrees of freedom, e.g., physical spins or particles in a many-body system. They may also represent population counts (as in a chemical master equation), indicator functions for macrostates, coarse-grained projections, or other types of variables.

The system’s stochastic dynamics over sequences of $T + 1$

discrete timesteps are described by a “forward” trajectory distribution $p(\vec{\mathbf{x}})$, where each trajectory $\vec{\mathbf{x}} = (\mathbf{x}_0, \mathbf{x}_1, \dots, \mathbf{x}_T)$ is a sequence of $T + 1$ states. In general, $T = 1$ suffices for stationary first-order-Markovian systems, while larger T may describe non-Markovian and non-stationary systems. The system is also associated with a “reverse” trajectory distribution $\tilde{p}(\vec{\mathbf{x}})$. The *trajectory EP* of trajectory $\vec{\mathbf{x}}$ and the *average EP* across all trajectories are defined as [1]

$$\sigma(\vec{\mathbf{x}}) := \ln \frac{p(\vec{\mathbf{x}})}{\tilde{p}(\vec{\mathbf{x}})}, \quad \Sigma := D(p\|\tilde{p}) = \left\langle \ln \frac{p(\vec{\mathbf{x}})}{\tilde{p}(\vec{\mathbf{x}})} \right\rangle_p, \quad (1)$$

where $\langle \dots \rangle_p = \sum_{\vec{\mathbf{x}}} \dots p(\vec{\mathbf{x}})$ is the expectation over p and $D(\cdot\|\cdot)$ is the Kullback-Leibler (KL) divergence. EP quantifies the violation of time-reversal symmetry, and it vanishes in equilibrium when trajectory statistics are indistinguishable under the forward and reverse distributions.

Our goal is to estimate $\sigma(\vec{\mathbf{x}})$ and Σ using samples of empirical trajectories from the forward and backward distributions. For simplicity, we mostly focus on the common case of stationary systems without odd variables (such as velocity). In this case, $\tilde{p}(\vec{\mathbf{x}}) = p(\vec{\mathbf{x}})$, where $\vec{\mathbf{x}} = (\mathbf{x}_T, \mathbf{x}_{T-1}, \dots, \mathbf{x}_0)$, and the statistics are invariant to time-shifting, so samples from the forward and reverse processes may be generated by dividing a long timeseries and its reversed version into sequences of size $T + 1$. However, our approach is more general, being compatible also with nonstationary and odd systems. In the general case, our method requires samples of multiple trajectories from separate forward and reverse processes.

EP decomposition.— For high-dimensional systems with many degrees of freedom (large N) or long memory (large T), the set of possible trajectories is exponentially large. In such cases, estimating trajectory probabilities $p(\vec{\mathbf{x}})$ from empirical data becomes statistically infeasible. This prevents estimation of trajectory-level and expected EP by direct evaluation of (1).

We propose a lower bound on EP based on a nonequilibrium generalization of the MaxEnt variational principle. We assume that we have access to d trajectory observables, represented

by a vector-valued function $\mathbf{g}(\vec{x}) \in \mathbb{R}^d$. Natural choices of observables include low-order interaction terms, such as 1-point $(x_{i,t})$ and 2-point $(x_{i,t}x_{j,t'})$ correlations. We do *not* require antisymmetric observables $\mathbf{g}(\vec{x}) = -\mathbf{g}(\vec{x})$.

To quantify the EP captured by the temporal irreversibility of observables \mathbf{g} , we find the distribution that has the smallest KL divergence to the reverse process, subject to having the same observable expectations as the forward process:

$$\Sigma_{\mathbf{g}} := \min_q D(q||\tilde{p}) \quad \text{subject to} \quad \langle \mathbf{g} \rangle_q = \langle \mathbf{g} \rangle_p. \quad (2)$$

$\Sigma_{\mathbf{g}}$ is always nonnegative, and it vanishes only when the expectation of \mathbf{g} is the same under the forward and reverse processes. Furthermore, it is straightforward to show that $\Sigma_{\mathbf{g}} \leq D(p_G||\tilde{p}_G) \leq \Sigma$, where $p_G(\mathbf{g}') = \sum_{\vec{x}} p(\vec{x})\delta_{\mathbf{g}',\mathbf{g}(\vec{x})}$ and $\tilde{p}_G(\mathbf{g}') = \sum_{\vec{x}} \tilde{p}(\vec{x})\delta_{\mathbf{g}',\mathbf{g}(\vec{x})}$ indicate the distributions of \mathbf{g} under the forward and backward processes (see *Supplemental Material* (SM) [16]). In general, estimating $D(p_G||\tilde{p}_G)$ is as difficult as estimating Σ , since it requires inference of the high-dimensional distributions p_G and \tilde{p}_G .

On the other hand, by exploiting a remarkable information-theoretic duality, we may calculate $\Sigma_{\mathbf{g}}$ without explicitly inferring any probability distributions. Specifically, as shown in the *End Matter*, the optimization problem (2) has the dual formulation

$$\Sigma_{\mathbf{g}} = \max_{\boldsymbol{\theta} \in \mathbb{R}^d} \left(\boldsymbol{\theta}^\top \langle \mathbf{g} \rangle_p - \ln \langle e^{\boldsymbol{\theta}^\top \mathbf{g}} \rangle_{\tilde{p}} \right). \quad (3)$$

Eq. (3) is a tractable convex optimization problem over the Lagrangian multipliers $\boldsymbol{\theta}$ that enforce the d expectation constraints on \mathbf{g} . Importantly, the objective depends only on the expectations of $\mathbf{g}(\vec{x})$ under p and $e^{\boldsymbol{\theta}^\top \mathbf{g}(\vec{x})}$ under \tilde{p} , which can be easily computed from empirical samples of the observables.

As an example, consider a system with 1000 binary spins measured at two timepoints. A naive estimate of Σ would require inference of $\sim 2^{1000}$ probabilities. Instead, with \mathbf{g} encoding 2-point correlations, Eq. (3) results in a tractable unconstrained optimization problem over $\sim 1000^2$ variables.

So far, we made no assumptions regarding multipartite structure (i.e., only a single variable can change at a time). However, as we show in *End Matter*, for multipartite dynamics and multipartite observables, Eq. (3) can be split into N separate optimization problems, each one involving only a proportional fraction of the variables and observations. This can dramatically reduce the amount of computation and memory required to numerically solve Eq. (3).

The distribution q^* that optimizes (2) lies in the exponential family,

$$q_{\boldsymbol{\theta}}(\vec{x}) = \tilde{p}(\vec{x}) e^{\boldsymbol{\theta}^\top \mathbf{g}(\vec{x}) - \ln \langle e^{\boldsymbol{\theta}^\top \mathbf{g}} \rangle_{\tilde{p}}}. \quad (4)$$

We can interpret the optimal $\boldsymbol{\theta}^*$ in Eq. (3) as the optimal parameters in the maximum likelihood (ML) problem $\boldsymbol{\theta}^* = \arg \min_{\boldsymbol{\theta}} D(p||q_{\boldsymbol{\theta}})$, since $q_{\boldsymbol{\theta}^*} = q^*$ satisfies the constraints in (2) and achieves the optimum objective value (see *End*

Matter). This interpretation also leads to the information-geometric Pythagorean theorem [17], which decomposes EP into two nonnegative KL terms:

$$\underbrace{D(p||\tilde{p})}_{\Sigma} = \underbrace{D(q^*||\tilde{p})}_{\Sigma_{\mathbf{g}}} + \underbrace{D(p||q^*)}_{\Sigma_{\mathbf{g}}^\perp}. \quad (5)$$

The term $\Sigma_{\mathbf{g}}^\perp := \Sigma - \Sigma_{\mathbf{g}} = D(p||q^*)$ quantifies the EP not captured by $\Sigma_{\mathbf{g}}$. It can be expressed in terms of a ML problem, $\Sigma_{\mathbf{g}}^\perp = \min_{\boldsymbol{\theta} \in \mathbb{R}^d} D(p||q_{\boldsymbol{\theta}})$. To interpret this expression, we define a larger exponential family $\omega_f(\vec{x}) := \tilde{p}(\vec{x})e^{f(\vec{x})}/\langle e^f \rangle_{\tilde{p}}$ that contains the forward trajectory distribution $p(\vec{x}) = \omega_\sigma(\vec{x})$. The ML problem can be written as

$$\Sigma_{\mathbf{g}}^\perp = \min_{\boldsymbol{\theta} \in \mathbb{R}^d} D(\omega_\sigma||\omega_{\boldsymbol{\theta}^\top \mathbf{g}}). \quad (6)$$

From this expression, it is clear that $\Sigma_{\mathbf{g}}^\perp = 0$ (and $\Sigma_{\mathbf{g}} = \Sigma$) if and only if trajectory EP is a linear combination of the trajectory observables, i.e., $\sigma(\vec{x}) = \boldsymbol{\theta}^{*\top} \mathbf{g}(\vec{x})$ for all \vec{x} . When $\Sigma_{\mathbf{g}}^\perp > 0$, $\boldsymbol{\theta}^{*\top} \mathbf{g}(\vec{x})$ provides the best possible approximation of $\sigma(\vec{x})$ in the span of \mathbf{g} .

Eq. (4) implies that the conditional distribution of the optimal q^* obeys $q_{\vec{x}|G}^*(\vec{x}|\mathbf{g}') = \tilde{p}_{\vec{x}|G}(\vec{x}|\mathbf{g}')$, with conditional probabilities given by Bayes' rule, $p_{\vec{x}|G}(\vec{x}|\mathbf{g}') = p(\vec{x})\delta_{\mathbf{g}',\mathbf{g}(\vec{x})}/p_G(\mathbf{g}')$. Using the chain rule of KL divergence, we may further decompose $\Sigma_{\mathbf{g}}^\perp$ into

$$\Sigma_{\mathbf{g}}^\perp = D(p_G||q_G^*) + D(p_{\vec{x}|G}||\tilde{p}_{\vec{x}|G}). \quad (7)$$

The first term in Eq. (7) vanishes when $q_G^* = p_G$; it is the additional EP that could be inferred by constraining all higher-order statistics (not just the mean) in Eq. (2). The second term is the EP that cannot be inferred from any statistics of \mathbf{g} .

Finally, our method supports a hierarchical decomposition of EP, where contributions from interactions of increasing order (e.g., pairwise, triplets) are successively added, resulting in a structure $0 \leq \Sigma_1 \leq \Sigma_2 \leq \dots \leq \Sigma$, with $\Sigma_k = D(q_k^*||\tilde{p})$ capturing contributions from functions $\mathbf{g}(\vec{x})$ containing interactions up to order k . This structure mirrors information-geometric decompositions in equilibrium MaxEnt [17, 18] and allows EP to be broken down into interpretable components, each satisfying $\Sigma_k - \Sigma_{k-1} = D(q_k^*||q_{k-1}^*)$.

Thermodynamic uncertainty relations (TURs).— Eq. (3) can be interpreted as a TUR that relates EP and fluctuations of trajectory observables [19]. Consider any trajectory observable that can be expressed as a linear combination $o(\vec{x}) = \boldsymbol{\theta}^\top \mathbf{g}(\vec{x})$ for some $\boldsymbol{\theta} \in \mathbb{R}^d$. The first term in (3) is the expectation of $o(\vec{x})$, while the second term is the cumulant generating function (CGF) of $o(\vec{x})$ under \tilde{p} . Thus, $\Sigma_{\mathbf{g}}$ bounds the “fluctuation discounted” expectation of all such $o(\vec{x})$, giving a higher-order TUR [14] that constrains all cumulants of trajectory observables. This contrasts with quadratic TURs, which constrain only the mean and variance [20–22].

To relate our approach to quadratic TURs, we expand the CGF as $\ln \langle e^{\boldsymbol{\theta}^\top \mathbf{g}} \rangle_{\tilde{p}} \approx \boldsymbol{\theta}^\top \langle \mathbf{g} \rangle_{\tilde{p}} + \boldsymbol{\theta}^\top \mathbf{K}_{\tilde{p}} \boldsymbol{\theta} / 2$, where $\mathbf{K}_{\tilde{p}}$ is the covariance matrix of \mathbf{g} under \tilde{p} . Plugging into (3) gives the

approximate optimizer $\hat{\theta}$ as the solution to the linear system $K_{\tilde{p}}\theta = \langle \mathbf{g} \rangle_p - \langle \mathbf{g} \rangle_{\tilde{p}} \equiv \langle \mathbf{g} \rangle_{p-\tilde{p}}$. This gives the weaker bound

$$\Sigma_{\mathbf{g}} \geq \hat{\Sigma}_{\mathbf{g}} := \langle \mathbf{g} \rangle_{p-\tilde{p}}^{\top} K_{\tilde{p}}^{-1} \langle \mathbf{g} \rangle_p - \ln \left\langle e^{\langle \mathbf{g} \rangle_{p-\tilde{p}}^{\top} K_{\tilde{p}}^{-1} \mathbf{g}} \right\rangle_{\tilde{p}}. \quad (8)$$

$\hat{\Sigma}_{\mathbf{g}}$ can be shown to correspond to a single Newton-Raphson step for maximizing (3) starting from $\theta = \mathbf{0}$ [16]; it has the advantage of not requiring optimization, only the solution a linear system. The bound $\Sigma_{\mathbf{g}} \geq \hat{\Sigma}_{\mathbf{g}}$ becomes tight when \mathbf{g} has Gaussian statistics.

We may also compare our results to a quadratic TUR. For stationary systems without odd variables, we find the inequality (see *End Matter*)

$$\Sigma \geq \Sigma_{\mathbf{g}}^{\text{TUR}} := \frac{1}{2} (\langle \mathbf{g} \rangle_p - \langle \mathbf{g} \rangle_{\tilde{p}})^{\top} K_{(p+\tilde{p})/2}^{-1} (\langle \mathbf{g} \rangle_p - \langle \mathbf{g} \rangle_{\tilde{p}}) \quad (9)$$

where $K_{(p+\tilde{p})/2}$ is the covariance matrix of \mathbf{g} under the mixture distribution $(p + \tilde{p})/2$. For antisymmetric observables, Eq. (9) may be considered the discrete-time version of the multidimensional TUR from Ref. [22].

The bounds (8)-(9) may require solving linear systems involving very large covariance matrices. For multipartite systems, it is often possible to split these bounds into N bounds that involve smaller matrices (see *End Matter*).

Related work.— Eq. (3) is closely related to the Donsker-Varadhan representation from large deviations theory [23], previously used to estimate information-theoretic quantities in machine learning [24] and thermodynamic inference [25–27]. However, these works did not consider the problem of thermodynamic inference in high-dimensional systems using multivariate observables. Other approaches to EP inference have employed compression algorithms [28–30] and deep learning of probability flows [31].

Our Pythagorean theorem (5) is related to previous decompositions of EP in interacting systems [32] and systems with nonconservative forces [15, 33, 34]. Moreover, the general form of Eq. (2) is a Maximum Entropy (MaxEnt) problem over trajectory distributions [35–38], sometimes called “maximum caliber” (MaxCal) [39]. Related techniques have been used to infer models from which the entropy flow can be estimated, though without ensuring a lower bound [40].

Our approach differs in several other ways from earlier work on MaxEnt and MaxCal. First, we minimize the KL divergence relative to an unknown prior distribution \tilde{p} , from which we typically only have some samples. This makes standard approximation methods for large-scale MaxEnt problems (such as mean-field and Bethe approximations [6, 41, 42]) not directly applicable. Second, we care not only about the parameters θ , as is typical of MaxEnt “inverse problems”, but also about bounding EP by the quantity $\Sigma_{\mathbf{g}}$. Both of these issues are resolved by the dual formulation (3).

Lynn et al. [12, 43, 44] proposed a way to decompose and bound EP using a different information-theoretic optimization. Although originally focused on local EP in multipartite stationary systems, it can be generalized to arbitrary observables \mathbf{g}

and non-multipartite systems as

$$\Sigma_{\mathbf{g}}^{\text{L}} = \min_{q, \tilde{q}} D(q \| \tilde{q}) \quad \text{subject to} \quad \langle \mathbf{g} \rangle_q = \langle \mathbf{g} \rangle_p. \quad (10)$$

Here we use assumption of stationarity and no odd variables, so that $\tilde{q}(\tilde{\mathbf{x}}) = q(\tilde{\mathbf{x}})$. Like our bound $\Sigma_{\mathbf{g}}$, $\Sigma_{\mathbf{g}}^{\text{L}}$ can be used to generate hierarchical decompositions of EP.

Although Eq. (10) resembles Eq. (2), it differs in that it simultaneously optimizes both arguments of the KL divergence, q and \tilde{q} . As we discuss in the *End Matter*, the optimal distribution q^* in Eq. (10) is not in an exponential family and in general it lacks full support. For this reason, Eq. (10) does not have a tractable dual expression (i.e., analogous to our dual (3)), and there is no straightforward way to scale $\Sigma_{\mathbf{g}}^{\text{L}}$ to large systems.

Examples: Nonequilibrium spin model and Neuropixels dataset.— We illustrate our approach using two examples: a nonequilibrium kinetic Ising model [6, 45, 46], and *in vivo* spike data from the Neuropixels Visual Behavior repository [47]. In both systems, we focus on a single time step and binary variables $x_{i,t} \in \{-1, +1\}$, $i \in \{1, \dots, N\}$ with time $t \in \{0, 1\}$, and assume stationarity.

To calculate $\Sigma_{\mathbf{g}}$, we optimize Eq. (3) using gradient ascent with Barzilai–Borwein step sizes [48]. We perform early-stopping using held-out validation data, which avoids overfitting even in the far-from-equilibrium regime where many reverse transitions are not sampled. Reported EP estimates are computed on held-out test data. Details of the data generation, optimization, and analysis are found in the SM [16] and our code repository [49].

The nonequilibrium spin model is specified by transition probabilities

$$T(\mathbf{x}_1 | \mathbf{x}_0) = \frac{1}{N} \sum_i \left[W_i(\mathbf{x}_0) \delta_{\mathbf{x}_0, \mathbf{x}_1^{[i]}} + (1 - W_i(\mathbf{x}_0)) \delta_{\mathbf{x}_0, \mathbf{x}_1} \right]$$

Here we introduce the spin-flip operator, $(\mathbf{x}^{[i]})_i = -x_i$ and $(\mathbf{x}^{[i]})_j = x_j$ for $j \neq i$. The flip probability for spin i is

$$W_i(\mathbf{x}) = \frac{\exp(-\beta x_i \sum_{j:j \neq i} w_{ij} x_j)}{2 \cosh(\beta \sum_{j:j \neq i} w_{ij} x_j)}, \quad (11)$$

where β is an inverse temperature and w_{ij} are (typically asymmetric) coupling parameters. We consider the diluted version of the model [50–52] with k average neighbors. Here $w_{ij} = c_{ij} z_{ij} / \sqrt{k}$, with binary connections $c_{ij} \sim \text{Bernoulli}(k/(N-1))$ and real-valued weights $z_{ij} \sim \mathcal{N}(0, 1)$.

The steady-state EP in this model has a simple closed-form expression, $\Sigma = \beta \sum_{i \neq j} w_{ij} \langle (x_{i,1} - x_{i,0}) x_{j,0} \rangle_{\text{st}}$, where $\langle \cdot \rangle_{\text{st}}$ indicates expectations under the stationary process p . This provides ground truth to evaluate our estimators.

Our observables of interest are time-lagged correlations,

$$g_{ij}(\tilde{\mathbf{x}}) = (x_{i,1} - x_{i,0}) x_{j,0} \quad \text{for all } i, j, \quad (12)$$

with conjugate parameters θ_{ij} . Because the system has multipartite dynamics and observables, Eq. (3) can be decomposed

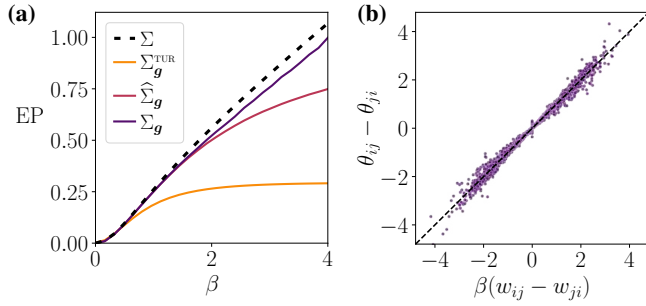


FIG. 1. Disordered nonequilibrium spin model with 1000 spins. **(a)** Steady-state EP estimates for different inverse temperatures β . **(b)** Asymmetry of inferred parameters, shown against the true coupling asymmetries in the model for $\beta = 2.5$ ($R^2 = 0.9831$). Estimates are based on 10^9 state transitions sampled by Monte Carlo.

into N independent problems, each involving only those transitions where spin i changes, improving computational performance for large systems.

Fig. 1(a) shows the actual and inferred EP at different β for $N = 1000$, $k = 6$. EP increases with β , and all estimators (Σ_g^{TUR} , $\widehat{\Sigma}_g$, Σ_g) agree in the near-equilibrium regime of small β . Importantly, Σ_g provides a tight bound on EP even in the far-from-equilibrium regime of large β . The gap between Σ_g and $\widehat{\Sigma}_g$ indicates the onset of highly non-Gaussian statistics from $\beta \approx 2$.

As discussed near Eq. (6), $\Sigma_g \approx \Sigma$ implies that the trajectory EP $\sigma(\vec{x})$ can be closely approximated by a linear combination of observables g_{ij} . As shown in the SM, our optimal parameters θ^* can be used to infer the asymmetry of the coupling constants, $\theta_{ij}^* - \theta_{ji}^* \approx \beta(w_{ij} - w_{ji})$. This relation is verified in Fig. 1(b).

In the SM, we also consider a different family of coupling matrices, for which this model exhibits a nonequilibrium phase transition [6]. We show that our approach accurately infers EP in this regime, a difficult task for existing approximations [53].

Next, as an example application to biological data, we estimate EP in the Visual Behavior Neuropixels dataset [47], containing spike-train recordings from 81 mice across 103 sessions. EP is here interpreted as a statistical measure of time-irreversibility, not energetic dissipation [13]. The dataset includes spiking activity from multiple brain regions, including visual cortical areas (VISp, VISl, VISal, VISrl, VISam and VISpm) and subcortical structures. We analyze data from visual areas during three conditions: active behavior (visual change detection task), passive replay (same stimuli but without task engagement), and Gabor (receptive field characterization with Gabor stimuli and full-field flashes). We discretize spike trains into temporal bins of length $\Delta t = 10$ ms and verify that most bins contain no more than one spike. We note that neurons can update in a parallel (non-multipartite) manner.

Our observables are defined as

$$g_{ij}(\vec{x}) = x_{i,1}x_{j,0} - x_{i,0}x_{j,1} \quad \text{for all } i < j, \quad (13)$$

which naturally represent time-lagged correlations in non-

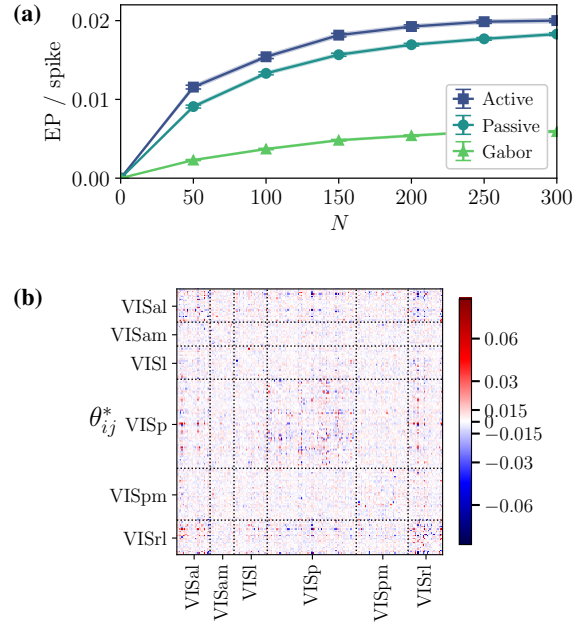


FIG. 2. **(a)** Estimated EP per expected number of spikes R , in the Neuropixels *Visual Behavior* dataset for three conditions. Error bars indicate standard error of the mean. **(b)** A sample of inferred coupling coefficients θ_{ij}^* , grouped by visual area. Here we select 200 neurons with highest firing rate from an active trial. To improve visualization, lower triangle shows $\theta_{ji}^* \equiv -\theta_{ij}^*$ for $i < j$.

multipartite dynamics. They capture the antisymmetric part of (12) and give more robust numerical results on this dataset.

We calculate EP estimates across different conditions and system sizes N . For each combination of size, condition, and recording session, we randomly select 10 subsets of neurons and estimate Σ_g for each subset. For improved comparison, we normalize EP in each condition by the expected number of spikes per bin, $R = \sum_i (1 + \langle x_{i,0} \rangle_{st}) / 2$.

Fig. 2(a) shows that EP grows superlinearly with size (note that $R \propto N$). It also shows that the active condition is associated with the largest normalized EP. Fig. 2(b) illustrates the matrix of inferred parameters θ_{ij}^* for 200 neurons from an active trial, grouped by visual brain area. These parameters can be understood as the coupling coefficients that best describe temporal irreversibility of the *in vivo* neural dynamics. Notably, they reveal a clustered organization that is aligned with anatomical brain regions.

AUTHOR CONTRIBUTIONS

A.K. and M.A. contributed equally to this work.

ACKNOWLEDGEMENTS

M.A. is partly supported by John Templeton Foundation (grant 62828) and Grant PID2023-146869NA-I00 funded by MICIU/AEI/10.13039/501100011033 and cofunded by the

European Union, and supported by the Basque Government through the BERC 2022-2025 program and by the Spanish State Research Agency through BCAM Severo Ochoa excellence accreditation CEX2021-01142-S funded by MICIU/AEI/10.13039/501100011033. S. I. is supported by JSPS KAKENHI Grants No. 22H01141, No. 23H00467, and No. 24H00834, JST ERATO Grant No. JPMJER2302, and UTEC-UTokyo FSI Research Grant Program. A.K. is partly supported by John Templeton Foundation (grant 62828) and by the European Union's Horizon 2020 research and innovation programme under the Marie Skłodowska-Curie Grant Agreement No. 101068029.

DATA AVAILABILITY STATEMENT

The code used in this study is available at a GitHub repository [49].

* Corresponding authors: artemyk@gmail.com, maguilera@bcamath.org. These authors contributed equally to this work.

- [1] U. Seifert, Stochastic thermodynamics, fluctuation theorems and molecular machines, *Reports on progress in physics* **75**, 126001 (2012).
- [2] G. Gallavotti and E. G. D. Cohen, Dynamical ensembles in nonequilibrium statistical mechanics, *Physical review letters* **74**, 2694 (1995).
- [3] J. Kurchan, Fluctuation theorem for stochastic dynamics, *Journal of Physics A: Mathematical and General* **31**, 3719 (1998).
- [4] C. Maes, The fluctuation theorem as a Gibbs property, *Journal of statistical physics* **95**, 367 (1999).
- [5] C. Jarzynski, Hamiltonian derivation of a detailed fluctuation theorem, *Journal of Statistical Physics* **98**, 77 (2000).
- [6] M. Aguilera, M. Igarashi, and H. Shimazaki, Nonequilibrium thermodynamics of the asymmetric Sherrington-Kirkpatrick model, *Nature Communications* **14**, 3685 (2023).
- [7] C. Battle, C. P. Broedersz, N. Fakhri, V. F. Geyer, J. Howard, C. F. Schmidt, and F. C. MacKintosh, Broken detailed balance at mesoscopic scales in active biological systems, *Science* **352**, 604 (2016).
- [8] T. H. Tan, A. Mietke, J. Li, Y. Chen, H. Higinbotham, P. J. Foster, S. Gokhale, J. Dunkel, and N. Fakhri, Odd dynamics of living chiral crystals, *Nature* **607**, 287 (2022).
- [9] C. W. Lynn, E. J. Cornblath, L. Papadopoulos, M. A. Bertolero, and D. S. Bassett, Broken detailed balance and entropy production in the human brain, *Proceedings of the National Academy of Sciences* **118**, e2109889118 (2021).
- [10] L. A. de la Fuente, F. Zamberlan, H. Bocaccio, M. Kringelbach, G. Deco, Y. S. Perl, C. Pallavicini, and E. Tagliazucchi, Temporal irreversibility of neural dynamics as a signature of consciousness, *Cerebral Cortex* **33**, 1856 (2023).
- [11] D. Sekizawa, S. Ito, and M. Oizumi, Decomposing thermodynamic dissipation of linear Langevin systems via oscillatory modes and its application to neural dynamics, *Physical Review X* **14**, 041003 (2024).
- [12] S. M. Geli, C. W. Lynn, M. L. Kringelbach, G. Deco, and Y. S. Perl, Non-equilibrium whole-brain dynamics arise from pairwise interactions, *Cell Reports Physical Science* (2025).
- [13] R. Nartallo-Kaluarachchi, M. L. Kringelbach, G. Deco, R. Lambiotte, and A. Goriely, Nonequilibrium physics of brain dynamics, *arXiv preprint arXiv:2504.12188* (2025).
- [14] A. Dechant and S.-i. Sasa, Fluctuation–response inequality out of equilibrium, *Proceedings of the National Academy of Sciences* **117**, 6430 (2020).
- [15] A. Kolchinsky, A. Dechant, K. Yoshimura, and S. Ito, Generalized free energy and excess entropy production for active systems, *arXiv preprint arXiv:2412.08432* (2024).
- [16] See Supplemental Material at [URL will be inserted by publisher] for a detailed description of the Newthorn-Raphson method results and the nonequilibrium spin model and the Neuropixels spike train examples.
- [17] S.-I. Amari, Information geometry on hierarchy of probability distributions, *IEEE transactions on information theory* **47**, 1701 (2001).
- [18] N. Ay, Information geometry on complexity and stochastic interaction, *Entropy* **17**, 2432 (2015).
- [19] J. M. Horowitz and T. R. Gingrich, Thermodynamic uncertainty relations constrain non-equilibrium fluctuations, *Nature Physics* **16**, 15 (2020).
- [20] J. Li, J. M. Horowitz, T. R. Gingrich, and N. Fakhri, Quantifying dissipation using fluctuating currents, *Nature communications* **10**, 1666 (2019).
- [21] S. K. Manikandan, D. Gupta, and S. Krishnamurthy, Inferring entropy production from short experiments, *Physical review letters* **124**, 120603 (2020).
- [22] A. Dechant, Multidimensional thermodynamic uncertainty relations, *Journal of Physics A: Mathematical and Theoretical* **52**, 035001 (2018).
- [23] M. D. Donsker and S. S. Varadhan, Asymptotic evaluation of certain Markov process expectations for large time, i, *Communications on pure and applied mathematics* **28**, 1 (1975).
- [24] M. I. Belghazi, A. Baratin, S. Rajeswar, S. Ozair, Y. Bengio, A. Courville, and R. D. Hjelm, MINE: Mutual Information Neural Estimation, *arXiv preprint arXiv:1801.04062* (2018).
- [25] D.-K. Kim, Y. Bae, S. Lee, and H. Jeong, Learning entropy production via neural networks, *Physical Review Letters* **125**, 140604 (2020).
- [26] S. Otsubo, S. K. Manikandan, T. Sagawa, and S. Krishnamurthy, Estimating time-dependent entropy production from non-equilibrium trajectories, *Communications Physics* **5**, 11 (2022).
- [27] T. GrandPre, K. Klymko, K. K. Mandadapu, and D. T. Limmer, Entropy production fluctuations encode collective behavior in active matter, *Physical Review E* **103**, 012613 (2021).
- [28] É. Roldán and J. M. Parrondo, Estimating dissipation from single stationary trajectories, *Physical review letters* **105**, 150607 (2010).
- [29] É. Roldán and J. M. Parrondo, Entropy production and Kullback-Leibler divergence between stationary trajectories of discrete systems, *Physical Review E—Statistical, Nonlinear, and Soft Matter Physics* **85**, 031129 (2012).
- [30] S. Ro, B. Guo, A. Shih, T. V. Phan, R. H. Austin, D. Levine, P. M. Chaikin, and S. Martiniani, Model-free measurement of local entropy production and extractable work in active matter, *Physical review letters* **129**, 220601 (2022).
- [31] N. M. Boffi and E. Vanden-Eijnden, Deep learning probability flows and entropy production rates in active matter, *Proceedings of the National Academy of Sciences* **121**, e2318106121 (2024).
- [32] S. Ito, M. Oizumi, and S.-i. Amari, Unified framework for the entropy production and the stochastic interaction based on information geometry, *Physical Review Research* **2**, 033048 (2020).

- [33] S. Ito, Geometric thermodynamics for the Fokker–Planck equation: stochastic thermodynamic links between information geometry and optimal transport, *Information geometry* **7**, 441 (2024).
- [34] A. Kolchinsky, A. Dechant, K. Yoshimura, and S. Ito, Information geometry of excess and housekeeping entropy production, arXiv preprint arXiv:2206.14599 (2022).
- [35] A. Tang, D. Jackson, J. Hobbs, W. Chen, J. L. Smith, H. Patel, A. Prieto, D. Petrusca, M. I. Grivich, A. Sher, *et al.*, A maximum entropy model applied to spatial and temporal correlations from cortical networks in vitro, *Journal of Neuroscience* **28**, 505 (2008).
- [36] O. Marre, S. El Boustani, Y. Frégnac, and A. Destexhe, Prediction of spatiotemporal patterns of neural activity from pairwise correlations, *Physical review letters* **102**, 138101 (2009).
- [37] H. C. Nguyen, R. Zecchina, and J. Berg, Inverse statistical problems: from the inverse Ising problem to data science, *Advances in Physics* **66**, 197 (2017).
- [38] R. Cofré and C. Maldonado, Information entropy production of maximum entropy Markov chains from spike trains, *Entropy* **20**, 34 (2018).
- [39] K. Ghosh, P. D. Dixit, L. Agozzino, and K. A. Dill, The maximum caliber variational principle for nonequilibria, *Annual review of physical chemistry* **71**, 213 (2020).
- [40] K. Ishihara and H. Shimazaki, State-space kinetic Ising model reveals task-dependent entropy flow in sparsely active nonequilibrium neuronal dynamics, arXiv preprint arXiv:2502.15440 (2025).
- [41] M. Welling and Y. W. Teh, Approximate inference in Boltzmann machines, *Artificial Intelligence* **143**, 19 (2003).
- [42] F. Ricci-Tersenghi, The Bethe approximation for solving the inverse Ising problem: a comparison with other inference methods, *Journal of Statistical Mechanics: Theory and Experiment* **2012**, P08015 (2012).
- [43] C. W. Lynn, C. M. Holmes, W. Bialek, and D. J. Schwab, Decomposing the local arrow of time in interacting systems, *Physical review letters* **129**, 118101 (2022).
- [44] C. W. Lynn, C. M. Holmes, W. Bialek, and D. J. Schwab, Emergence of local irreversibility in complex interacting systems, *Physical Review E* **106**, 034102 (2022).
- [45] A. Crisanti and H. Sompolinsky, Dynamics of spin systems with randomly asymmetric bonds: Ising spins and Glauber dynamics, *Physical Review A* **37**, 4865 (1988).
- [46] H. Eissfeller and M. Opper, Mean-field Monte Carlo approach to the Sherrington-Kirkpatrick model with asymmetric couplings, *Physical Review E* **50**, 709 (1994).
- [47] A. I. for Brain Science, *Allen Brain Observatory: Visual Behavior Neuropixels Technical Whitepaper v1.0 – 8.16.22*, whitepaper (Allen Institute for Brain Science, 2022).
- [48] R. Fletcher, On the Barzilai-Borwein method, in *Optimization and control with applications* (Springer, 2005) pp. 235–256.
- [49] M. Aguilera and A. Kolchinsky, **Inferring entropy production in many-body systems using nonequilibrium MaxEnt: Code repository** (2025).
- [50] A. Coolen, Statistical mechanics of recurrent neural networks II—Dynamics, in *Handbook of biological physics*, Vol. 4 (Elsevier, 2001) pp. 619–684.
- [51] E. Aurell and H. Mahmoudi, A message-passing scheme for non-equilibrium stationary states, *Journal of Statistical Mechanics: Theory and Experiment* **2011**, P04014 (2011).
- [52] P. Zhang, Inference of kinetic Ising model on sparse graphs, *Journal of Statistical Physics* **148**, 502 (2012).
- [53] M. Aguilera, S. A. Moosavi, and H. Shimazaki, A unifying framework for mean-field theories of asymmetric kinetic Ising systems, *Nature communications* **12**, 1197 (2021).
- [54] S. Boyd, *Convex optimization*, Cambridge UP (2004).
- [55] E. L. Lehmann and G. Casella, *Theory of point estimation* (Springer Science & Business Media, 2006).
- [56] G. Tripathi, A matrix extension of the Cauchy-Schwarz inequality, *Economics Letters* **63**, 1 (1999).

END MATTER

Derivation of Eq. (3).— We consider the MaxEnt problem (2) associated with the Lagrangian

$$\mathcal{L}(q, \boldsymbol{\theta}, \lambda) = D(q\|\tilde{p}) + \boldsymbol{\theta}^\top (\langle \mathbf{g} \rangle_p - \langle \mathbf{g} \rangle_q) + \lambda(1 - \langle 1 \rangle_q),$$

where $\boldsymbol{\theta} \in \mathbb{R}^d$ enforces the expectation constraints and $\lambda \in \mathbb{R}$ enforces the normalization constraint ($\langle 1 \rangle_q = \sum_{\vec{x}} q(\vec{x}) = 1$). We do not have to include Lagrange multipliers for the non-negativity constraints $q(\vec{x}) \geq 0$ because, as we show below, the optimal distribution will always be in an exponential family and have the same support as \tilde{p} .

To find the critical points of the Lagrangian, we take the gradient of \mathcal{L} with respect to $q(\vec{x})$ and set to 0,

$$1 + \ln q^*(\vec{x}) - \ln \tilde{p}(\vec{x}) - \boldsymbol{\theta}^\top \mathbf{g}(\vec{x}) - \lambda = 0, \quad (14)$$

giving the solution $q^*(\vec{x}) = \tilde{p}(\vec{x}) e^{\boldsymbol{\theta}^\top \mathbf{g}(\vec{x}) - \lambda - 1}$. The multiplier λ is determined by the normalization condition $\langle 1 \rangle_{q^*} = 1$ and can be eliminated, yielding the exponential-family form

$$q^*(\vec{x}) = q_{\boldsymbol{\theta}}(\vec{x}) = \tilde{p}(\vec{x}) e^{\boldsymbol{\theta}^\top \mathbf{g}(\vec{x}) - \ln \langle e^{\boldsymbol{\theta}^\top \mathbf{g}} \rangle_{\tilde{p}}}. \quad (15)$$

The constrained optimization (2) can be written in terms of the Lagrangian as

$$\Sigma_{\mathbf{g}} = \min_q \max_{\boldsymbol{\theta}, \lambda} \mathcal{L}(q, \boldsymbol{\theta}, \lambda). \quad (16)$$

Because the objective in (2) is convex and p is a feasible point on the relative interior of the feasible set, we may use convex duality [54] to write this optimization as

$$\Sigma_{\mathbf{g}} = \max_{\boldsymbol{\theta}, \lambda} \min_q \mathcal{L}(q, \boldsymbol{\theta}, \lambda). \quad (17)$$

The inner optimization can be solved to give (15), which can be plugged back into (17) and simplified to give Eq. (3). The exponential-family distribution $q_{\boldsymbol{\theta}^*}$ for the optimal parameters $\boldsymbol{\theta}^*$ is also the optimizer of the MaxEnt problem (2).

The optimal $\boldsymbol{\theta}^*$ in Eq. (3) may also be derived by considering maximum likelihood (ML) in the exponential family (15),

$$\boldsymbol{\theta}^* = \arg \min_{\boldsymbol{\theta}} D(p\|q_{\boldsymbol{\theta}}). \quad (18)$$

To see why, observe that the objective of the ML problem is convex and that the optimal $\boldsymbol{\theta}^*$ satisfies $\mathbf{0} = \nabla_{\boldsymbol{\theta}} D(p\|q_{\boldsymbol{\theta}})|_{\boldsymbol{\theta}=\boldsymbol{\theta}^*} = \langle \mathbf{g} \rangle_p - \langle \mathbf{g} \rangle_{q_{\boldsymbol{\theta}^*}}$. This implies that $q_{\boldsymbol{\theta}^*}$ satisfies the expectation constraints in (2) while also being at a critical point of the Lagrangian (14). Therefore, it must be the optimizer of the MaxEnt problem (2).

Multipartite systems.— For multipartite systems, the optimization problem (3) can often be decomposed into a set of smaller problems. For simplicity, we consider a single timestep ($T = 1$) of a discrete system. We also assume multipartite dynamics and multipartite observables. For dynamics, this means that only a single variable $i \in \{1, \dots, N\}$ changes

at any one time, $p(\vec{x}) = \tilde{p}(\vec{x}) = 0$ whenever both $x_{i,0} \neq x_{i,1}$ and $x_{j,0} \neq x_{j,1}$ are satisfied for $i \neq j$. For observables, the multipartite assumption means that \mathbf{g} can be partitioned as

$$\mathbf{g} = (\mathbf{g}_0, \mathbf{g}_1, \dots, \mathbf{g}_N, \mathbf{a}), \quad (19)$$

Here \mathbf{g}_i for $i \in \{1, \dots, N\}$ specifies observables that reflect changes of variable i ($\mathbf{g}_i(\mathbf{x}_0, \mathbf{x}_1) = \mathbf{0}$ if $x_{i,0} = x_{i,1}$), while \mathbf{g}_0 specifies observables that reflect the state not changing ($\mathbf{g}_0(\mathbf{x}_0, \mathbf{x}_1) = \mathbf{0}$ if $\mathbf{x}_0 \neq \mathbf{x}_1$). The observables $\mathbf{a} = (a_0, a_1, \dots, a_N)$ are indicator functions for changes of variable i , $a_i(\mathbf{x}_0, \mathbf{x}_1) = 1 - \delta_{x_{i,0}, x_{i,1}}$. The presence of these indicator observables is an assumption, though not a very strong one as such observables can usually be easily added if not already present in \mathbf{g} . We also define $a_0(\mathbf{x}_0, \mathbf{x}_1) := 1 - \sum_{i=1}^N a_i(\mathbf{x}_0, \mathbf{x}_1)$ as the indicator function for the state not changing.

Let $P_i := \langle a_i \rangle_p$ indicate the probability that variable i changes under the forward process, and $p_i(\vec{x}) := a_i(\vec{x})p(\vec{x})/P_i$ the forward distribution conditioned on change of i . Similarly, $P_0 := \langle a_0 \rangle_p$ and $p_0(\vec{x}) := a_0(\vec{x})p(\vec{x})/P_0$ indicate the probability and conditional distribution of trajectories where the state does not change. \tilde{P}_i and \tilde{p}_i indicate the same quantities under the reverse process \tilde{p} , and Q_i and q_i under a generic trajectory distribution q . Typically, the probabilities P_i and \tilde{P}_i can be easily estimated from empirical frequencies.

We recall our variational principle (2),

$$\Sigma_{\mathbf{g}} = \min_q D(q\|\tilde{p}) \quad \text{subject to} \quad \langle \mathbf{g} \rangle_q = \langle \mathbf{g} \rangle_p. \quad (20)$$

Without loss of generality, we may restrict the optimization to distributions q with the same multipartite structure, because any q that assigns a strictly positive probability to a non-multipartite transition (more than one variable changes state) has support outside of \tilde{p} and therefore $D(q\|\tilde{p}) = \infty$. Given multipartite q and \tilde{p} , we condition the trajectory distributions on which variable i , if any, undergoes a change. The chain rule for KL divergence then gives

$$D(q\|\tilde{p}) = D(Q\|\tilde{P}) + \sum_{i=0}^N Q_i D(q_i\|\tilde{p}_i), \quad (21)$$

where $D(Q\|\tilde{P}) = \sum_{i=0}^N Q_i \ln(Q_i/\tilde{P}_i)$.

Given our assumption of multipartite dynamics and observables, we have $\langle \mathbf{g}_i \rangle_q = Q_i \langle \mathbf{g}_i \rangle_{q_i}$ and $\langle \mathbf{g}_i \rangle_p = P_i \langle \mathbf{g}_i \rangle_{p_i}$. Also, the constraint $\langle \mathbf{a} \rangle_q = \langle \mathbf{a} \rangle_p$ implied by Eq. (20) means that $Q_i = P_i$. Combining allows us to decompose $\Sigma_{\mathbf{g}}$ as

$$\Sigma_{\mathbf{g}} = D(P\|\tilde{P}) + \sum_{i=0}^N P_i \Sigma_{\mathbf{g}}^{(i)}, \quad (22)$$

where we introduced the subproblem $i \in \{0, \dots, N\}$ as

$$\Sigma_{\mathbf{g}}^{(i)} := \min_{q_i} D(q_i\|\tilde{p}_i) \quad \text{subject to} \quad \langle \mathbf{g}_i \rangle_{q_i} = \langle \mathbf{g}_i \rangle_{p_i}. \quad (23)$$

Note that $\langle \mathbf{a} \rangle_{q_i} = \langle \mathbf{a} \rangle_{p_i}$ and $\langle \mathbf{g}_j \rangle_{q_i} = \langle \mathbf{g}_j \rangle_{p_i}$ for $j \neq i$ are automatically satisfied in the subproblem, and so can be dropped from the optimization. Each subproblem yields an exponential-form solution and a dual representation,

$$\Sigma_{\mathbf{g}}^{(i)} = \max_{\boldsymbol{\theta}_i} \left(\boldsymbol{\theta}_i^\top \langle \mathbf{g}_i \rangle_{p_i} - \ln \langle e^{\boldsymbol{\theta}_i^\top \mathbf{g}_i} \rangle_{\tilde{p}_i} \right). \quad (24)$$

where $\boldsymbol{\theta}_i$ are the parameters conjugate to \mathbf{g}_i .

Although our decomposition increases the number of optimization problems, each optimization problem is (typically $\sim N$ times) smaller than Eq. (3), both in terms of the number of optimization variables and the number of data points used to estimate conditional expectations under p_i and \tilde{p}_i . Furthermore, we may bound each $\Sigma_{\mathbf{g}}^{(i)}$ using the optimization-free bound $\widehat{\Sigma}_{\mathbf{g}}^{(i)}$ using a smaller covariance matrix than in Eq. (8).

Next, we consider the trajectory EP for multipartite systems. For any trajectory \vec{x} , we may write the trajectory EP as

$$\sigma(\vec{x}) := \ln \frac{p(\vec{x})}{\tilde{p}(\vec{x})} = \sum_{i=0}^N a_i(\vec{x}) \left[\ln \frac{P_i}{\tilde{P}_i} + \ln \frac{p_i(\vec{x})}{\tilde{p}_i(\vec{x})} \right]. \quad (25)$$

Observe that $\Sigma_{\mathbf{g}} \rightarrow \Sigma$ only if $\Sigma_{\mathbf{g}}^{(i)} \rightarrow \Sigma^{(i)}$ for each i . Then, using a maximum likelihood expression similar to Eq. (6), we may show that $\Sigma_{\mathbf{g}}^{(i)} = \Sigma^{(i)}$ implies

$$\ln \frac{p_i(\vec{x})}{\tilde{p}_i(\vec{x})} = \boldsymbol{\theta}_i^{*\top} \mathbf{g}_i(\vec{x}). \quad (26)$$

Combining Eqs. (25)-(26) and $a_i(\vec{x})\mathbf{g}_i(\vec{x}) = \mathbf{g}_i(\vec{x})$ gives

$$\sigma(\vec{x}) = \sum_{i=0}^N \left[a_i(\vec{x}) \ln \frac{P_i}{\tilde{P}_i} + \boldsymbol{\theta}_i^{*\top} \mathbf{g}_i(\vec{x}) \right]. \quad (27)$$

For a steady-state system without odd variables, $P_i = \langle a_i \rangle_p = \langle a_i \rangle_{\tilde{p}} = \tilde{P}_i$ since $p(\vec{x}) = \tilde{p}(\vec{x})$ and $a_i(\vec{x})$ is symmetric under time reversal. We also have $p_0 = \tilde{p}_0$, which allows us to ignore the no-change terms corresponding to $i = 0$. In this case, our results simplify to

$$\Sigma_{\mathbf{g}} = \sum_{i=1}^N P_i \Sigma_{\mathbf{g}}^{(i)} \quad (28)$$

$$\sigma(\vec{x}) = \sum_{i=1}^N \boldsymbol{\theta}_i^{*\top} \mathbf{g}_i(\vec{x}) \quad \text{when} \quad \Sigma_{\mathbf{g}} = \Sigma. \quad (29)$$

Finally, for these systems, we may derive a decomposed version of the multidimensional TUR (9) by bounding each term in $\Sigma = \sum_{i=1}^N P_i \Sigma^{(i)}$, where $\Sigma^{(i)} = D(p_i \| \tilde{p}_i)$ is the EP due to changes of variable i .

Multidimensional TUR (9).— For a stationary system without odd variables, $\tilde{p}(\vec{x}) = p(\vec{x})$, letting us write the EP as

$$\Sigma = \sum_{\vec{x}} p(\vec{x}) \ln \frac{p(\vec{x})}{p(\vec{x})} = \frac{1}{2} \sum_{\vec{x}} [p(\vec{x}) - p(\vec{x})] \ln \frac{p(\vec{x})}{p(\vec{x})}.$$

For continuous-state systems, sums should be replaced by integrals. Using the inequality $(a-b) \ln(a/b) \geq 2(a-b)^2/(a+b)$ for nonnegative a and b , we get the quadratic bound

$$\Sigma \geq \sum_{\vec{x}} \frac{(p(\vec{x}) - p(\vec{x}))^2}{p(\vec{x}) + p(\vec{x})}. \quad (30)$$

Next, for convenience, we define the symmetrized distribution $\mu(\vec{x}) = [p(\vec{x}) + p(\vec{x})]/2 = [p(\vec{x}) + \tilde{p}(\vec{x})]/2$ and the function $v(\vec{x}) := [p(\vec{x}) - \tilde{p}(\vec{x})]/\mu(\vec{x})$. Then, for any vector $\boldsymbol{\alpha}$,

$$\boldsymbol{\alpha}^\top (\langle \mathbf{g} \rangle_p - \langle \mathbf{g} \rangle_{\tilde{p}}) = \boldsymbol{\alpha}^\top \langle \mathbf{g} v \rangle_{\mu} = \boldsymbol{\alpha}^\top \langle \mathbf{g} v \rangle_{\mu} - \boldsymbol{\alpha}^\top \langle \mathbf{g} \rangle_{\mu} \langle v \rangle_{\mu},$$

where we used that $\langle v \rangle_{\mu} = 0$. Defining the centered observable $\mathbf{g}'(\vec{x}) := \mathbf{g}(\vec{x}) - \langle \mathbf{g} \rangle_{\mu}$, we write

$$\begin{aligned} (\boldsymbol{\alpha}^\top (\langle \mathbf{g} \rangle_p - \langle \mathbf{g} \rangle_{\tilde{p}}))^2 &= (\boldsymbol{\alpha}^\top \langle \mathbf{g}' v \rangle_{\mu})^2 \\ &\leq \langle (\boldsymbol{\alpha}^\top \mathbf{g}')_{\mu} \langle v^2 \rangle_{\mu} = (\boldsymbol{\alpha}^\top \langle \mathbf{g}' \mathbf{g}'^\top \rangle_{\mu} \boldsymbol{\alpha}) \langle v^2 \rangle_{\mu}, \end{aligned}$$

where we used the Cauchy-Schwarz inequality. Note that $\langle v^2 \rangle_{\mu} \leq 2\Sigma$ from Eq. (30) and that $\langle \mathbf{g}' \mathbf{g}'^\top \rangle_{\mu} \equiv \mathbf{K}_{\mu} \equiv \mathbf{K}_{(p+\tilde{p})/2}$. Plugging $\boldsymbol{\alpha} = \mathbf{K}_{\mu}^{-1} (\langle \mathbf{g} \rangle_p - \langle \mathbf{g} \rangle_{\tilde{p}})$ into the above inequality and rearranging gives the multidimensional TUR (9).

This result can also be derived from Eq. (30) by using the Hammersley-Chapman-Robbins bound [55, p. 114] or the matrix version of the Cauchy-Schwarz inequality [56].

Comparison with Lynn et al. [44].— We consider the optimization problem that defines $\Sigma_{\mathbf{g}}^L$ (10), our generalization of Ref. [44]. For a stationary system without odd variables, $\tilde{q}(\vec{x}) = q(\vec{x})$ and the partial derivative of the objective with respect to $\tilde{q}(\vec{x})$ is

$$\partial_{q(\vec{x})} D(q \| \tilde{q}) = 1 + \ln \frac{q(\vec{x})}{\tilde{q}(\vec{x})} - \frac{\tilde{q}(\vec{x})}{q(\vec{x})}.$$

Observe that this expression does not diverge even when a pair of probabilities $q(\vec{x})$ and $\tilde{q}(\vec{x})$ are taken to zero. Therefore, in general, the optimal distribution in Eq. (10) may not have full support, and will instead lay on the boundary of the set of probability distributions. By considering some numerical examples, we have verified that the optimization (10) often returns solutions without full support.

For comparison, the partial derivative of our MaxEnt objective (2), $\partial_{q(\vec{x})} D(q \| \tilde{p}) = 1 + \ln[q(\vec{x})/\tilde{p}(\vec{x})]$ diverges to $-\infty$ as $q(\vec{x}) \rightarrow 0$ for any \vec{x} where $\tilde{p}(\vec{x}) \geq 0$. This implies that a point on the boundary cannot be the minimizer, thus the optimal solution will lie in the relative interior of the feasible set.

This difference has significant consequences for the tractability of the two optimization problems. The fact that strict positivity is enforced by our objective (2) allows us to restate the optimization in terms of a tractable dual problem (3). On the other hand, the dual formulation of (10) requires an exponential number of nonnegative Lagrange multipliers, one for each pair of trajectories \vec{x} and \tilde{x} to guarantee nonnegativity of $q(\vec{x})$ and $q(\tilde{x})$. Therefore, the dual formulation of (10) involves an intractable constrained optimization problem over an exponential number of parameters.

SUPPLEMENTAL MATERIAL

Here we provide more details of our derivations, methods, and the two examples considered in the paper: the nonequilibrium spin model and the Neuropixels spike dataset.

SM 1. COARSE-GRAINED KL DIVERGENCE BOUNDS

For clarity, in this section we explicitly indicate trajectory distributions like p, \tilde{p}, q, \dots with subscripts like $p_{\vec{x}}, \tilde{p}_{\vec{x}}, q_{\vec{x}}, \dots$. We denote by $\mathbf{g}(\vec{x})$ the vector of d observables associated with each trajectory \vec{x} . Given distribution $p_{\vec{x}}$, we use the notation $p_{\vec{x}G}(\vec{x}, \mathbf{g}') = p_{\vec{x}}(\vec{x})\delta_{\mathbf{g}', \mathbf{g}(\vec{x})}$ to indicate the associated joint distribution over trajectories and observables (and similarly for other distributions like $\tilde{p}_{\vec{x}G}, q_{\vec{x}G}, \dots$). Such joint distributions induce marginal distributions over observables, $p_G(\mathbf{g}') = \sum_{\vec{x}} p_{\vec{x}}(\vec{x})\delta_{\mathbf{g}', \mathbf{g}(\vec{x})}$, as well as corresponding conditional distributions $p_{\vec{x}|G}$ and $p_{G|\vec{x}}$, computed according to usual rules of probability calculus. For continuous-state systems, sums should be replaced by integrals and the Kronecker delta by the Dirac delta.

Let us consider the optimization problem that defines $\Sigma_{\mathbf{g}}$,

$$\Sigma_{\mathbf{g}} := \min_q D(q_{\vec{x}} \| \tilde{p}_{\vec{x}}) \quad \text{subject to} \quad \langle \mathbf{g}(\vec{x}) \rangle_{q_{\vec{x}}} = \langle \mathbf{g}(\vec{x}) \rangle_{p_{\vec{x}}}. \quad (\text{S1})$$

We introduce the trajectory distribution $q'_{\vec{x}}(\vec{x}) := p_G(\mathbf{g}(\vec{x}))\tilde{p}_{\vec{x}|G}(\vec{x}|\mathbf{g}(\vec{x}))$. It is easy to verify by marginalization that $q'_{\vec{x}}$ satisfies the constraint $\langle \mathbf{g}(\vec{x}) \rangle_{q'_{\vec{x}}} = \langle \mathbf{g}(\vec{x}) \rangle_{p_{\vec{x}}}$, thus $\Sigma_{\mathbf{g}} \leq D(q'_{\vec{x}} \| \tilde{p}_{\vec{x}})$. We also have the identities

$$\begin{aligned} D(q'_{\vec{x}} \| \tilde{p}_{\vec{x}}) &= D(q'_{\vec{x}} \| \tilde{p}_{\vec{x}G}) + D(q'_{G|\vec{x}} \| \tilde{p}_{G|\vec{x}}) \\ &= D(q'_{\vec{x}G} \| \tilde{p}_{\vec{x}G}) = D(p_G \tilde{p}_{\vec{x}|G} \| \tilde{p}_G \tilde{p}_{\vec{x}|G}) \\ &= D(p_G \| \tilde{p}_G) + D(\tilde{p}_{\vec{x}|G} \| \tilde{p}_{\vec{x}|G}) = D(p_G \| \tilde{p}_G). \end{aligned}$$

In the first line, we used $D(q'_{G|\vec{x}} \| \tilde{p}_{G|\vec{x}}) = 0$ since $q'_{G|\vec{x}}(\mathbf{g}'|\vec{x}) = \tilde{p}_{G|\vec{x}}(\mathbf{g}'|\vec{x}) = \delta_{\mathbf{g}', \mathbf{g}(\vec{x})}$; in the second line, we used the chain rule of KL divergence and the definition of $q'_{\vec{x}}$; in the last line, we again used the chain rule of KL divergence. Furthermore, by the data processing inequality [1], the KL divergence between trajectory distributions satisfies the inequality $\Sigma = D(p_{\vec{x}} \| \tilde{p}_{\vec{x}}) \geq D(p_G \| \tilde{p}_G)$. This follows from the fact that the observable map $\mathbf{g}(\vec{x})$ is a (potentially many-to-one) function of the trajectory \vec{x} , which constitutes a form of coarse-graining. Combining these results, we obtain the following chain of inequalities:

$$\Sigma_{\mathbf{g}} \leq D(p_G \| \tilde{p}_G) \leq D(p_{\vec{x}} \| \tilde{p}_{\vec{x}}) = \Sigma. \quad (\text{S2})$$

SM 2. OPTIMIZATION DETAILS

A. Gradient ascent

We used gradient ascent to optimize our objective (3) and generate the results for the nonequilibrium spin model and the Neuropixels dataset. In gradient ascent, the parameters are updated iteratively as

$$\boldsymbol{\theta}_{k+1} = \boldsymbol{\theta}_k + \alpha_k \nabla L(\boldsymbol{\theta}_k), \quad (\text{S3})$$

where α_k is the step size. The gradient of the objective $L(\boldsymbol{\theta}) = \boldsymbol{\theta}^\top \langle \mathbf{g} \rangle_p - \ln \langle e^{\boldsymbol{\theta}^\top \mathbf{g}} \rangle_{\tilde{p}}$ from Eq. (3) is

$$\nabla L(\boldsymbol{\theta}) = \langle \mathbf{g} \rangle_p - \langle \mathbf{g} \rangle_{q_\theta}. \quad (\text{S4})$$

Here $\langle \mathbf{g} \rangle_{q_\theta}$ is the expectation of \mathbf{g} under distribution $q_\theta(\vec{\mathbf{x}}) = \tilde{p}(\vec{\mathbf{x}}) e^{\boldsymbol{\theta}^\top \mathbf{g}(\vec{\mathbf{x}}) - \ln \langle e^{\boldsymbol{\theta}^\top \mathbf{g}} \rangle_{\tilde{p}}}$,

$$\langle g_n \rangle_{q_\theta} = \frac{\langle e^{\boldsymbol{\theta}^\top \mathbf{g}(\vec{\mathbf{x}})} g_n(\vec{\mathbf{x}}) \rangle_{\tilde{p}}}{\langle e^{\boldsymbol{\theta}^\top \mathbf{g}(\vec{\mathbf{x}})} \rangle_{\tilde{p}}}. \quad (\text{S5})$$

We used $\boldsymbol{\theta}_0 = \mathbf{0}$ and $\alpha_0 = 1/N$ as the starting parameters of the optimization (N is the dimensionality of the system).

We chose the step sizes according to the ‘‘short step’’ Barzilai–Borwein rule [2, 3],

$$\alpha_k = \frac{(\boldsymbol{\theta}_k - \boldsymbol{\theta}_{k-1})^\top (\nabla L(\boldsymbol{\theta}_k) - \nabla L(\boldsymbol{\theta}_{k-1}))}{\|\nabla L(\boldsymbol{\theta}_k) - \nabla L(\boldsymbol{\theta}_{k-1})\|^2}. \quad (\text{S6})$$

This rule estimates curvature information using previous iterations, without requiring explicit Hessian computations. It often leads to fast convergence on convex optimization problems.

To prevent overfitting, we employed a standard holdout strategy. The data was randomly split into 70% for training, 20% for validation, and 10% for testing. The training set was used to estimate the gradients of the objective. Optimization was halted once the objective on the validation set failed to improve for 10 consecutive iterations (early stopping). In addition, to prevent overfitting, optimization was also halted when estimated EP in training or validation was larger than $\ln n_{\text{samples}}$, where n_{samples} is number of samples. This cutoff was based on the observation that there is not enough data to reliably estimate KL divergence values larger than $\ln n_{\text{samples}}$ from datasets of size n_{samples} or smaller. We selected the parameters $\boldsymbol{\theta}^*$ that achieved the highest validation objective during training, and used these to evaluate the objective on a held-out test set, which we report as the final estimate of entropy production. This procedure gave reliable results and prevented overfitting, even in the far-from-equilibrium regime where some reverse transitions were too rare to be observed in realistic sample sizes.

B. Newton-Raphson optimization

The bound $\widehat{\Sigma}_{\mathbf{g}}$ from Eq. (8) can be interpreted in terms of Newton-Raphson optimization. To see this, note that the Newton-Raphson update for maximizing an objective function $L(\boldsymbol{\theta})$ is

$$\boldsymbol{\theta}_{k+1} = \boldsymbol{\theta}_k - (\nabla^2 L(\boldsymbol{\theta}_k))^{-1} \nabla L(\boldsymbol{\theta}_k). \quad (\text{S7})$$

For the objective $L(\boldsymbol{\theta}) = \boldsymbol{\theta}^\top \langle \mathbf{g} \rangle_p - \ln \langle e^{\boldsymbol{\theta}^\top \mathbf{g}} \rangle_{\tilde{p}}$, the gradient is given by Eq. (S4). The Hessian is $\nabla^2 L(\boldsymbol{\theta}) = -\mathbf{K}_{q_{\boldsymbol{\theta}}}$, the covariance of \mathbf{g} under distribution $q_{\boldsymbol{\theta}}(\vec{\mathbf{x}}) = \tilde{p}(\vec{\mathbf{x}}) e^{\boldsymbol{\theta}^\top \mathbf{g}(\vec{\mathbf{x}}) - \ln \langle e^{\boldsymbol{\theta}^\top \mathbf{g}} \rangle_{\tilde{p}}}$,

$$(\mathbf{K}_{q_{\boldsymbol{\theta}}})_{nm} = \langle g_n g_m \rangle_{q_{\boldsymbol{\theta}}} - \langle g_n \rangle_{q_{\boldsymbol{\theta}}} \langle g_m \rangle_{q_{\boldsymbol{\theta}}} = \frac{\langle e^{\boldsymbol{\theta}^\top \mathbf{g}(\vec{\mathbf{x}})} g_n(\vec{\mathbf{x}}) g_m(\vec{\mathbf{x}}) \rangle_{\tilde{p}}}{\langle e^{\boldsymbol{\theta}^\top \mathbf{g}(\vec{\mathbf{x}})} \rangle_{\tilde{p}}} - \langle g_n \rangle_{q_{\boldsymbol{\theta}}} \langle g_m \rangle_{q_{\boldsymbol{\theta}}} \quad (\text{S8})$$

Taking a single step from $\boldsymbol{\theta}_k = \mathbf{0}$ recovers $\widehat{\Sigma}_{\mathbf{g}}$ (8), because $\boldsymbol{\theta}_{k+1} = \mathbf{K}_{\tilde{p}}^{-1} (\langle \mathbf{g} \rangle_p - \langle \mathbf{g} \rangle_{\tilde{p}}) = \hat{\boldsymbol{\theta}}$.

SM 3. NONEQUILIBRIUM SPIN MODEL

A. Model and data generation

To define our nonequilibrium spin model, we randomly sample (and quench) the coupling parameters w_{ij} as a product of two independently sampled random variables: $w_{ij} = c_{ij} z_{ij} / \sqrt{k}$. Here, $z_{ij} \sim \mathcal{N}(0, 1)$ are Gaussian-distributed weights, while $c_{ij} \sim \text{Bernoulli}(k/(N-1))$ are binary variables that enforce sparsity by randomly selecting a subset of active connections. This construction yields a sparse network with quenched disorder. We use an average in-degree of $k = 6$.

We use Monte Carlo to draw $10^6 \times N$ samples from 10^3 independent restarts. Each restart begins on a random initial configuration and then undergoes a burn-in period of $10^5 \times N$ Glauber updates according to Eq. (11). For computational efficiency, for each visited configuration, we independently sample a Glauber update for each of the N spins before moving on to the next configuration. To reduce temporal correlations, we discard N Glauber steps between sampling intervals.

B. Optimization using multipartite assumption

The nonequilibrium spin model satisfies the assumptions of our multipartite analysis, as discussed in the *End Matter*. Specifically, the system is discrete and it is measured over a single timestep in steady state. In addition, the dynamics are multipartite, because only a single spin can change state at any one time. The observables (12) are multipartite because $g_{ij}(\vec{\mathbf{x}}) \neq 0$ only if spin i changes state in transition $\vec{\mathbf{x}}$.

Using these assumptions, we can solve the optimization problem $\Sigma_{\mathbf{g}}$ by splitting it into N independent subproblems $\Sigma_{\mathbf{g}}^{(i)}$, as in Eqs. (23)-(28). Under this mapping, the observables $\mathbf{g}(\vec{\mathbf{x}})$ are grouped into blocks,

$$\mathbf{g}_i = (g_{i,1}, \dots, g_{i,i-1}, g_{i,i+1}, \dots, g_{i,N}). \quad (\text{S9})$$

Note that each block i contains $(N - 1)$ observables (g_{ij} for all j such that $j \neq i$). We do not include a block like \mathbf{g}_0 because, in this example, there are no observables that are non-zero when the state does not change. The diagonal observables g_{ii} are proportional to the indicator function for flips of spin i ,

$$g_{ii}(\vec{\mathbf{x}}) = (x_{i,1} - x_{i,0})x_{i,0} = -2(1 - \delta_{x_{i,0}, x_{i,1}}) = -2a_i(\vec{\mathbf{x}}).$$

Thus, constraining the expectation of g_{ii} is equivalent to constraining expectation of a_i , as discussed in the *End Matter*.

Each subproblem involves an optimization over $N - 1$ parameters. For moderately sized N , in principle, the objective can be optimized using second-order methods such as Newton's method. In practice, we found that trust-region Newton optimization [4] gave results similar to gradient ascent with Barzilai–Borwein steps.

We also used the multipartite assumption to simplify computation of the multivariate TUR bound $\Sigma_{\mathbf{g}}^{\text{TUR}}$. Specifically, we bound each individual KL term $\Sigma^{(i)} = D(p_i || \tilde{p}_i)$ using Eq. (9), then took the expectation to get a bound on $\Sigma = \sum_i P_i \Sigma^{(i)}$.

C. Steady-state EP

The steady-state EP is computed using the steady-state distribution, which satisfies $p^{\text{st}}(\mathbf{x}_1) = \sum_{\mathbf{x}_0} T(\mathbf{x}_1 | \mathbf{x}_0) p^{\text{st}}(\mathbf{x}_0)$. In steady state, the forward and reverse trajectory distributions are

$$p(\vec{\mathbf{x}}) = T(\mathbf{x}_1 | \mathbf{x}_0) p^{\text{st}}(\mathbf{x}_0) \quad \tilde{p}(\vec{\mathbf{x}}) = T(\mathbf{x}_0 | \mathbf{x}_1) p^{\text{st}}(\mathbf{x}_1)$$

Using these distributions, we may compute the EP as

$$\begin{aligned} \Sigma &= D(p || \tilde{p}) = \sum_{\mathbf{x}_0, \mathbf{x}_1} p^{\text{st}}(\mathbf{x}_0) T(\mathbf{x}_1 | \mathbf{x}_0) \ln \frac{p^{\text{st}}(\mathbf{x}_0) T(\mathbf{x}_1 | \mathbf{x}_0)}{p^{\text{st}}(\mathbf{x}_1) T(\mathbf{x}_0 | \mathbf{x}_1)} \\ &= \sum_{\mathbf{x}_0, \mathbf{x}_1} p^{\text{st}}(\mathbf{x}_0) T(\mathbf{x}_1 | \mathbf{x}_0) \ln \frac{T(\mathbf{x}_1 | \mathbf{x}_0)}{T(\mathbf{x}_0 | \mathbf{x}_1)} \\ &= \sum_{\mathbf{x}_0} \sum_i p^{\text{st}}(\mathbf{x}_0) T(\mathbf{x}_0^{[i]} | \mathbf{x}_0) \ln \frac{T(\mathbf{x}_0^{[i]} | \mathbf{x}_0)}{T(\mathbf{x}_0 | \mathbf{x}_0^{[i]})} \end{aligned} \quad (\text{S10})$$

In the second line, we used that the change of Shannon entropy vanishes in steady state,

$$\sum_{\mathbf{x}_0, \mathbf{x}_1} p^{\text{st}}(\mathbf{x}_0) T(\mathbf{x}_1 | \mathbf{x}_0) \ln \frac{p^{\text{st}}(\mathbf{x}_0)}{p^{\text{st}}(\mathbf{x}_1)} = \sum_{\mathbf{x}_0} p^{\text{st}}(\mathbf{x}_0) \ln p^{\text{st}}(\mathbf{x}_0) - \sum_{\mathbf{x}_1} p^{\text{st}}(\mathbf{x}_1) \ln p^{\text{st}}(\mathbf{x}_1) = 0.$$

In the third line, we used the multipartite structure of the dynamics.

Using Eq. (11) in the main text, the ratio of transition probabilities for trajectory $(\mathbf{x}_0, \mathbf{x}_0^{[i]})$ may be written as

$$\ln \frac{T(\mathbf{x}_0^{[i]} | \mathbf{x}_0)}{T(\mathbf{x}_0 | \mathbf{x}_0^{[i]})} = \ln \frac{W_i(\mathbf{x}_0)}{W_i(\mathbf{x}_0^{[i]})} = \beta \sum_{j:j \neq i} w_{ij} (x_{i,0}^{[i]} x_{j,0} - x_{i,0} x_{j,0}) \quad (\text{S11})$$

where we use $x_{i,0}^{[i]} = -x_{i,0}$ and cancel the $\cosh(\beta \sum_{j:j \neq i} w_{ij} x_{j,0})$ terms. Then, we may write the steady-state EP as

$$\begin{aligned} \Sigma &= \sum_{i \neq j} \sum_{\mathbf{x}_0} p^{\text{st}}(\mathbf{x}_0) T(\mathbf{x}_0^{[i]} | \mathbf{x}_0) \beta w_{ij} (x_{i,0}^{[i]} x_{j,0} - x_{i,0} x_{j,0}) \\ &= \sum_{i \neq j} \sum_{\mathbf{x}_0, \mathbf{x}_1} p^{\text{st}}(\mathbf{x}_0) T(\mathbf{x}_1 | \mathbf{x}_0) \beta w_{ij} (x_{i,1} x_{j,0} - x_{i,0} x_{j,0}) \end{aligned}$$

where we used that $x_{i,1} x_{j,0} - x_{i,0} x_{j,0} = 0$ for $\mathbf{x}_1 \neq \mathbf{x}_0^{[i]}$. Finally, introducing the notation $\langle \dots \rangle_{\text{st}} = \sum_{\mathbf{x}_0, \mathbf{x}_1} \dots p^{\text{st}}(\mathbf{x}_0) T(\mathbf{x}_1 | \mathbf{x}_0)$, we may write the steady-state EP as

$$\Sigma = \beta \sum_{i \neq j} w_{ij} \langle (x_{i,1} - x_{i,0}) x_{j,0} \rangle_{\text{st}}. \quad (\text{S12})$$

In terms of the observables \mathbf{g} (12), the steady-state EP may be expressed as $\Sigma = \beta \sum_{i \neq j} w_{ij} \langle g_{ij} \rangle_{\text{st}}$.

D. Relationship between coupling coefficients w_{ij} and parameters θ_{ij}^*

We now derive the relationship between the coupling coefficients w_{ij} and the optimal parameters θ_{ij}^* . We use the following expression for the trajectory EP of transition $\mathbf{x} \rightarrow \mathbf{x}^{[i]}$,

$$\sigma(\mathbf{x}, \mathbf{x}^{[i]}) = \ln \frac{T(\mathbf{x}^{[i]} | \mathbf{x}) p^{\text{st}}(\mathbf{x})}{T(\mathbf{x} | \mathbf{x}^{[i]}) p^{\text{st}}(\mathbf{x}^{[i]})} = -2\beta \sum_{j:j \neq i} w_{ij} x_i x_j + \ln \frac{p^{\text{st}}(\mathbf{x})}{p^{\text{st}}(\mathbf{x}^{[i]})}, \quad (\text{S13})$$

as follows from Eq. (S11) and $x_i^{[i]} = -x_i$.

We consider the sum of σ over a cyclic sequence of states $\mathbf{x} \rightarrow \mathbf{x}^{[i]} \rightarrow \mathbf{x}^{[i,k]} \rightarrow \mathbf{x}^{[k]} \rightarrow \mathbf{x}$, where

$\mathbf{x}^{[i,k]}$ indicates state \mathbf{x} with spins i and k flipped. For any initial \mathbf{x} and spins $i \neq k$, this gives

$$\sigma(\mathbf{x}, \mathbf{x}^{[i]}) + \sigma(\mathbf{x}^{[i]}, \mathbf{x}^{[i,k]}) + \sigma(\mathbf{x}^{[i,k]}, \mathbf{x}^{[k]}) + \sigma(\mathbf{x}^{[k]}, \mathbf{x}) \quad (\text{S14})$$

$$\begin{aligned} &= -2\beta \left[\sum_{j:j \neq i} w_{ij} x_i x_j + \sum_{j:j \neq k} w_{kj} x_k^{[i]} x_j^{[i]} + \sum_{j:j \neq i} w_{ij} x_i^{[i,k]} x_j^{[i,k]} + \sum_{j:j \neq k} w_{kj} x_k^{[k]} x_j^{[k]} \right] \\ &= -2\beta \left[\sum_{j:j \neq i} w_{ij} x_i x_j + \sum_{j:j \neq k} w_{kj} x_k x_j^{[i]} - \sum_{j:j \neq i} w_{ij} x_i x_j^{[i,k]} - \sum_{j:j \neq k} w_{kj} x_k x_j^{[k]} \right] \\ &= -2\beta \left[\sum_{j:j \neq i} w_{ij} x_i x_j + \sum_{j:j \neq k} w_{kj} x_k x_j^{[i]} - \sum_{j:j \neq i} w_{ij} x_i x_j^{[k]} - \sum_{j:j \neq k} w_{kj} x_k x_j \right] \\ &= -4\beta(w_{ik} - w_{ki})x_i x_k. \end{aligned} \quad (\text{S15})$$

The sum of the terms $\ln[p^{\text{st}}(\mathbf{x})/p^{\text{st}}(\mathbf{x}^{\prime})]$ cancels.

As shown in Fig. 1(a), our lower bound captures nearly all of EP, $\Sigma \approx \Sigma_g$. Therefore, given Eq. (29) in the *End Matter*, the trajectory EP for transition $\mathbf{x} \rightarrow \mathbf{x}^{[i]}$ can be expressed as

$$\sigma(\mathbf{x}, \mathbf{x}^{[i]}) \approx \sum_{i \neq j} \theta_{ij}^* g_{ij}(\mathbf{x}, \mathbf{x}^{[i]}), \quad (\text{S16})$$

for the optimal parameters θ^* . This expression does not include the diagonal observables $g_{ii} = -2a_i$, since they do not enter into the blocks \mathbf{g}_i in Eq. (S9). They are not included for the same reason that, in steady-state systems, the observables a_i do not enter into the calculation (29).

Plugging the observables \mathbf{g} from Eq. (12) into Eq. (S16) gives

$$\sigma(\mathbf{x}, \mathbf{x}^{[i]}) \approx \sum_{j:j \neq i} \theta_{ij}^* (x_i^{[i]} - x_i) x_j = -2 \sum_{j:j \neq i} \theta_{ij}^* x_i x_j. \quad (\text{S17})$$

Using this expression, we may write the sum (S14) in terms of our inferred parameters as

$$\begin{aligned} &\sigma(\mathbf{x}, \mathbf{x}^{[i]}) + \sigma(\mathbf{x}^{[i]}, \mathbf{x}^{[i,k]}) + \sigma(\mathbf{x}^{[i,k]}, \mathbf{x}^{[k]}) + \sigma(\mathbf{x}^{[k]}, \mathbf{x}) \\ &\approx -2 \left[\sum_{j:j \neq i} \theta_{ij}^* x_i x_j + \sum_{j:j \neq k} \theta_{kj}^* x_k^{[i]} x_j^{[i]} + \sum_{j:j \neq i} \theta_{ij}^* x_i^{[i,k]} x_j^{[i,k]} + \sum_{j:j \neq k} \theta_{kj}^* x_k^{[k]} x_j^{[k]} \right] \\ &= -2 \left[\sum_{j:j \neq i} \theta_{ij}^* x_i x_j + \sum_{j:j \neq k} \theta_{kj}^* x_k x_j^{[i]} - \sum_{j:j \neq i} \theta_{ij}^* x_i x_j^{[i,k]} - \sum_{j:j \neq k} \theta_{kj}^* x_k x_j^{[k]} \right] \\ &= -2 \left[\sum_{j:j \neq i} \theta_{ij}^* x_i x_j + \sum_{j:j \neq k} \theta_{kj}^* x_k x_j^{[i]} - \sum_{j:j \neq i} \theta_{ij}^* x_i x_j^{[k]} - \sum_{j:j \neq k} \theta_{kj}^* x_k x_j \right] \\ &= -4(\theta_{ik}^* - \theta_{ki}^*)x_i x_k. \end{aligned} \quad (\text{S18})$$

By comparing the two expressions, we have shown that for $i \neq k$,

$$\beta(w_{ik} - w_{ki}) \approx \theta_{ik}^* - \theta_{ki}^*. \quad (\text{S19})$$

E. Optimization-free inference of the EP phase transition in the asymmetric Sherrington-Kirkpatrick model

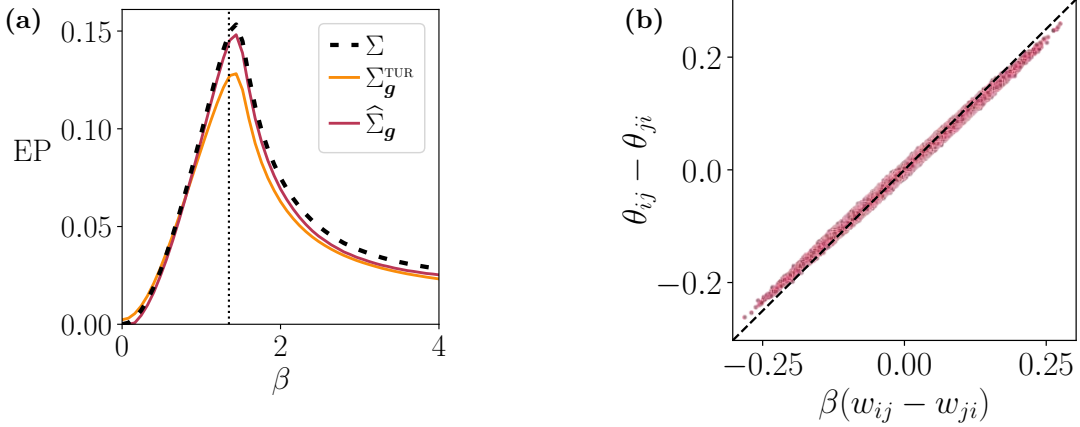


FIG. S1. (a) EP estimators $\Sigma_{\mathbf{g}}^{\text{TUR}}$ and $\widehat{\Sigma}_{\mathbf{g}}$ for the fully connected asymmetric Sherrington–Kirkpatrick model. (b) Inferred parameters corresponding to $\widehat{\Sigma}_{\mathbf{g}}$. Despite the presence of a critical point at $\beta \approx 1.3485$ (dotted line in (a)), where standard inference methods struggle [5], $\widehat{\Sigma}_{\mathbf{g}}$ accurately recovers the full EP.

To test the robustness of our estimator $\widehat{\Sigma}_{\mathbf{g}}$, we also evaluated it on a dense variant of the spin model. Specifically, we considered the case $k = N - 1$, where each spin is connected to all others. In this fully connected regime, the network converges to the asymmetric Sherrington–Kirkpatrick (SK) model, a classical mean-field model with quenched disorder and Gaussian couplings. We use a model with couplings $w_{ij} = w_0/N + \gamma z_{ij}/\sqrt{N}$, with $z_{ij} \sim \mathcal{N}(0, 1)$.

For $w_0 = 1$ and $\gamma = 1/2$, this model has a known ordered phase in the large- β limit, a second-order order-disorder critical point at $\beta \approx 1.3485$ where EP peaks [6]. Near the critical point, classical mean-field methods such as the TAP approximation fail in nonequilibrium MaxEnt parameter inference, leading to unreliable estimates of EP [5].

Figure S1 illustrates the results for the asymmetric SK model for $w_0 = 1, \gamma = 1/2$. We repeated our analysis using this dense coupling structure and found that $\widehat{\Sigma}_{\mathbf{g}}$ (with similar holdout methods as above) successfully recovered the full entropy production (EP). Although we do not plot it, we verified that $\Sigma_{\mathbf{g}}$ gives the same values. This demonstrates that our method performs reliably in disordered systems when the statistics approach a Gaussian distribution.

SM 4. NEUROPIXELS DATASET

We use high-resolution spiking data obtained from the Allen Institute’s Neuropixels dataset [7]. The dataset consists of multi-region neural recordings from awake mice, capturing parallel spike trains from hundreds of neurons simultaneously across brain areas.

A. Data selection and preprocessing

We use the AllenSDK Python library to download data and preprocess it to obtain binned binary spike trains for populations of neurons. For each session, we follow these steps:

- Session filtering: From 153 recorded sessions, we take the 103 sessions flagged as valid by default from the AllenSDK library.
- Unit filtering: We restrict the dataset to well-isolated units by applying standard quality control filters: signal-to-noise ratio (SNR) greater than 1, inter-spike interval (ISI) violations less than 1, and mean firing rate above 0.1 Hz. This ensures that only stable, active neurons are included.
- Spike binning: For each selected unit, we discretize its spike train using non-overlapping bins of 10 ms. This results in a high-dimensional binary time series with parallel (nonmultipartite) updates.
- Condition segmentation: Each recording session includes different behavioral and stimulus conditions, which are annotated in the Allen metadata. We define temporal masks to extract three conditions:
 1. Active behavior (60 min): periods where the animal was engaged in a visual discrimination task.
 2. Passive replay (60 min): periods when the animal passively viewed natural images.
 3. Gabor stimuli (25 min): control periods where drifting gratings (Gabor patches and full-field flashes) were shown instead of images.

Using the provided timestamps, we generate masks to extract the corresponding segments from the full spike train, yielding separate datasets for each condition. Under the selected bin size, each condition contains approximately 360,000 (active and passive) and 150,000 (Gabor) data points.

- Brain areas: Each unit is associated with a brain region via its recording channel. The dataset includes activity from visual cortical areas (VISp, VISl, VISal, VISrl, VISam and VISpm) as well as subcortical structures, such as the lateral geniculate nucleus, lateral posterior nucleus, hippocampus, and midbrain. We record these region labels alongside the spike data for the analysis shown in Fig. 2(b).

Optimization details

The Neuropixels dataset allows for parallel (nonmultipartite) transitions where multiple degrees of freedom change state at once. For this reason, we cannot factorize our optimization problem into independent problems as in Eq. (28) and the optimization involves a single problem with (up to) tens of thousands of parameters. Nonetheless, this problem can be solved relatively quickly using the gradient ascent method described above.

To ensure sufficient activity for reliable estimation, we only included neurons that were active in at least 2% of time bins. For each population size N , we averaged results across 10 independent trials, each using a different random subset of neurons. To visualize the inferred coupling parameters in Fig. 2(b), we selected 200 neurons with the highest firing rate from an active trial.

-
- [1] T. M. Cover, *Elements of information theory* (John Wiley & Sons, 1999).
 - [2] J. Barzilai and J. M. Borwein, Two-point step size gradient methods, *IMA journal of numerical analysis* **8**, 141 (1988).
 - [3] R. Fletcher, On the Barzilai-Borwein method, in *Optimization and control with applications* (Springer, 2005) pp. 235–256.
 - [4] C.-J. Lin and J. J. Moré, Newton’s method for large bound-constrained optimization problems, *SIAM Journal on Optimization* **9**, 1100 (1999).
 - [5] M. Aguilera, S. A. Moosavi, and H. Shimazaki, A unifying framework for mean-field theories of asymmetric kinetic Ising systems, *Nature communications* **12**, 1197 (2021).
 - [6] M. Aguilera, M. Igarashi, and H. Shimazaki, Nonequilibrium thermodynamics of the asymmetric Sherrington-Kirkpatrick model, *Nature Communications* **14**, 3685 (2023).
 - [7] A. I. for Brain Science, *Allen Brain Observatory: Visual Behavior Neuropixels Technical Whitepaper v1.0 – 8.16.22*, whitepaper (Allen Institute for Brain Science, 2022).